Antiferromagnetism in RuO_2 as d-wave Pomeranchuk instability

Kyo-Hoon Ahn,[1] Atsushi Hariki,[2] Kwan-Woo Lee,[1,3] and Jan Kuneš[2,4]
[1]*Division of Display and Semiconductor Physics, Korea University, Sejong 30019, Korea*
[2]*Institute of Solid State Physics, TU Wien, 1040 Vienna, Austria*
[3]*Department of Applied Physics, Graduate School, Korea University, Sejong 30019, Korea*
[4]*Institute of Physics, Czech Academy of Sciences, Na Slovance 2, 182 21 Praha 8, Czechia*

(Received 12 February 2019; revised manuscript received 10 April 2019; published 23 May 2019)

We present a computational study of antiferromagnetic transition in RuO_2. The rutile structure with the magnetic sublattices coupled with $\pi/2$ rotation leads to a spin-polarized band structure in the antiferromagnetic state, which gives rise to a d-wave modulation of the Fermi surface in the spin-triplet channel. We argue a finite spin conductivity that changes sign in the ab plane is expected in RuO_2 because of this band structure. We analyze the origin of the antiferromagnetic instability and link it to presence of a nodal line close to the Fermi level.

DOI: 10.1103/PhysRevB.99.184432

I. INTRODUCTION

Antiferromagnetic (AFM) metals have been attracting much interest recently because of their spintronic applications based on coupling between magnetic moments and charge current [1]. While ubiquitous among $3d$ transition metal oxides, antiferromagnetism in this group is typical for Mott insulators rather than metals. Metallic antiferromagnets can be found either doping Mott insulators as in cuprates, by replacing oxygen with more covalent ligands as in iron pnictides [2] or CuMnAs [3], or by moving down the periodic table to less correlated $4d$ transition metals. Itinerant antiferromagnetism, with magnetism and transport governed by the same electronic states, arises usually via the Slater mechanism [4]. Nesting between parts of the Fermi surface (FS) produces an instability that is resolved by an AFM state, which is stabilized by gapping the nested parts of FS.

The simplest—collinear—antiferromagnets have two magnetic sublattices with magnetic moments pointing in opposite directions. Reversing the sublattice magnetization, which amounts to exchanging the magnetic sublattices, generates a distinct AFM state which is typically indistinguishable by macroscopic measurements. This is the case when the magnetic sublattices are symmetry connected by a microscopic translation. In the reciprocal space, this is expressed by the spin-up and spin-down band structures being identical. Materials with even number of magnetic atoms in the unit cell allow AFM ordering without breaking of translation symmetry. The magnetic sublattices are then connected with some point group operation and spin-polarized band structure may arise. The recently studied CuMnAs [3], where magnetic sublattices are connected by inversion symmetry, is an example of such an antiferromagnet. However, in this case the spin polarization cannot be detected by inversion-invariant probes such as spin conductivity. It would be therefore interesting to have an AFM material with magnetic sublattices connected by rotation symmetry.

In this article, we show that rutile structure is suitable for this purpose and that ruthenium dioxide RuO_2, recently observed to be a room-temperature antiferromagnet [5,6], is a rare example of such a material. We report a computational study of RuO_2 using density functional theory plus dynamical mean-field theory (DFT+DMFT) as well as static Hartree-Fock (HF) techniques. We find that AFM order in RuO_2 leads to a spin-polarized band structure. The distinct spin-up and spin-down FSs are rotated by $\pi/2$ along the crystallographic c axis with respect to each other. The AFM order thus can be viewed as a d-wave Pomeranchuk instability in the spin-triplet channel [7]. We discuss the experimental implications and trace the origin of the AFM instability to a nodal line in the nonmagnetic (NM) band structure located in the vicinity of Fermi level.

II. COMPUTATIONAL METHOD

Starting from DFT electronic structure in the $P4_2/mnm$ structure [5] obtained with WIEN2K package [8], we constructed Wannier orbitals spanning the Ru $4d$ t_{2g} bands [9,10]. The tight-binding model was augmented by intra-atomic electron-electron interaction of the Slater-Kanamori form [11,12]

$$H_U = U\sum_{\alpha} n_{\alpha\uparrow}n_{\alpha\downarrow} + \sum_{\alpha>\beta,\sigma\sigma'}(U-2J-J\delta_{\sigma\sigma'})n_{\alpha\sigma}n_{\beta\sigma'} + \gamma J\sum_{\alpha\neq\beta}(c^{\dagger}_{\alpha\uparrow}c^{\dagger}_{\beta\downarrow}c_{\alpha\downarrow}c_{\beta\uparrow} + c^{\dagger}_{\alpha\uparrow}c^{\dagger}_{\alpha\downarrow}c_{\beta\downarrow}c_{\beta\uparrow} + \text{H.c.}),$$

where the indices α, β run over the orbital flavors on the same atom, whose site index was dropped for simplicity. The resulting Hubbard model was studied with DMFT and HF methods. The DMFT calculations employed the strong-coupling continuous-time quantum Monte Carlo method [13–16] and the density-density approximation ($\gamma = 0$) to H_U. HF calculations with spin-orbit coupling (SOC), included *a posteriori* to the mean-field Hamiltonian, were performed to determine the orientation of the local moments in the AFM state. The impact of SOC on the band structure was found to be only minor, in line with the conclusions of Ref. [17].

The calculations covered a wide range of U, J parameters and temperatures, as summarized in the Supplemental Material (SM) [18]. While size of the ordered moment varies with these parameters and among the two methods, the general observations presented here are shared by all calculations. Quantitatively, the DMFT and HF electronic structures corresponding to the same ordered moment agree with each other and as well as with DFT+U calculations, as shown in the SM [18]. This observation suggests that staggered Weiss field due to the AFM order, a feature shared by all methods, is the dominant effect. In the following, we present HF (DMFT) results for $U = 1.7$ (1.7) eV and $J = 0.2$ (0.45) eV at $T = 300$ (100) K.

III. RESULTS AND DISCUSSION

A. Spin-polarized band structure

In Fig. 1(a), we show the AFM band structure obtained with DMFT. The band structure throughout the Brillouin zone (BZ) is spin polarized, giving rise to a spin contrast shown in Fig. 1(b). Special high-symmetry planes, discussed below, are an exception where spin-up and spin-down bands are degenerate. In Fig. 1(c), we present NM and AFM bands obtained with the HF method. The ordered moment in the Wannier basis is $\approx 0.8\ \mu_B$ in both cases. Apart from noticeable dynamical bandwidth renormalization absent in the HF spectra, we observe overall a good agreement between the HF and DMFT results. This suggests that the weak-coupling HF approach provides a reasonable description of the physics of RuO_2 and we can use its simple structure to analyze the observed behavior.

Since both Ru_1 and Ru_2 sites with the antiparallel spin moments fit in the rutile unit cell, the AFM order does not affect the translation symmetry. It reduces the point symmetry, however. The operations connecting the magnetic sublattices (mapping Ru_1 to Ru_2), e.g., the 4_2 screw rotation, belong no more to the symmetry group. To do so, they must be augmented with spin inversion. As a result, the AFM band structure is spin polarized with the two spin channels being coupled by $\pi/2$ rotation. This distinguishes RuO_2 from other antiferromagnets with spin-polarized bands, such as tetragonal CuMnAs [3], where the magnetic sublattices, and thus the spin-polarized bands, are connected by inversion symmetry. The spin-up and spin-down bands of RuO_2 are degenerate (cross) along the $k_a = 0, \pi$ planes, which are invariant under the glide plane $x_a = 0$ connecting the magnetic sublattices. The same applies for $k_b = 0, \pi$ planes and $x_b = 0$ glide plane.

The spin polarized band structure gives rise to the FS shown in Fig. 2(b). The deformation of fourfold symmetric FS in Fig. 2(a) into a pair of two-fold symmetric FS connected by $\pi/2$ rotation and spin inversion can be classified as d-wave spin-triplet Pomeranchuk instability of the α type in the notation of Ref. [7]. This type of spin-polarized FS implies a finite longitudinal spin conductivity $\sigma_\uparrow - \sigma_\downarrow$ in the ab plane, with opposite signs in the (1,1,0) and (1,−1,0) directions, which vanishes along the crystallographic axes.

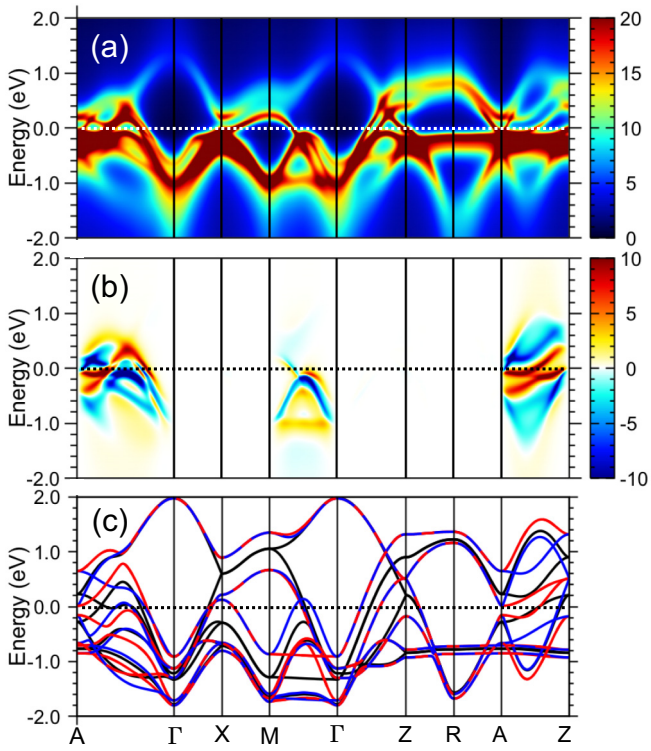

FIG. 1. (a) DFT+DMFT band structure, the spectral function $A_{\uparrow\uparrow}(\omega) + A_{\downarrow\downarrow}(\omega)$, along the high-symmetry lines in BZ. (b) The spin polarization of the band structure is calculated as $A_{\uparrow\uparrow}(\omega) - A_{\downarrow\downarrow}(\omega)$. (c) HF band structure: paramagnetic (black) and AFM (↑ red; ↓ blue). The energy is measured from the Fermi level.

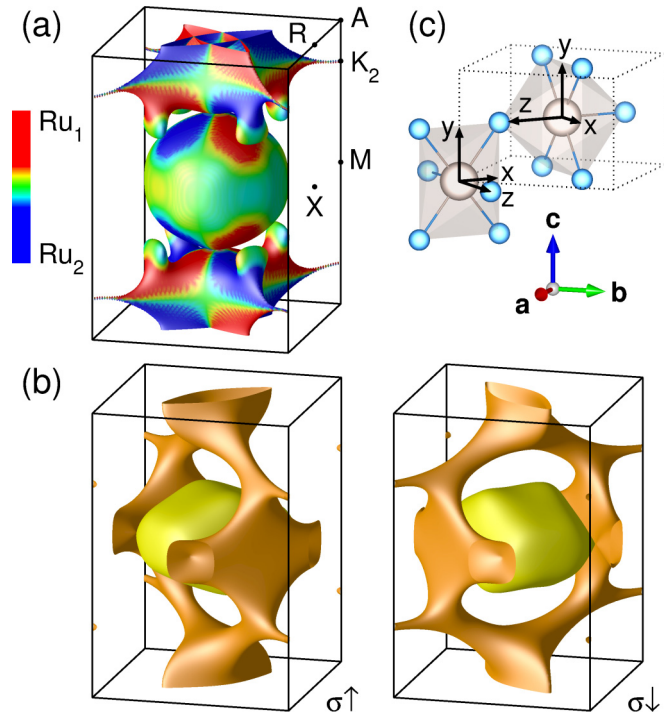

FIG. 2. (a) Fermi surface of paramagnetic RuO_2 obtained with HF method. The color codes the atomic polarization (difference of the Ru_1 and Ru_2 contributions to the wave function at a given k point). (b) Spin-polarized Fermi surface of the AFM state. (c) Crystal structure of RuO_2 with global, **a**, **b**, **c**, and local coordinates indicated.

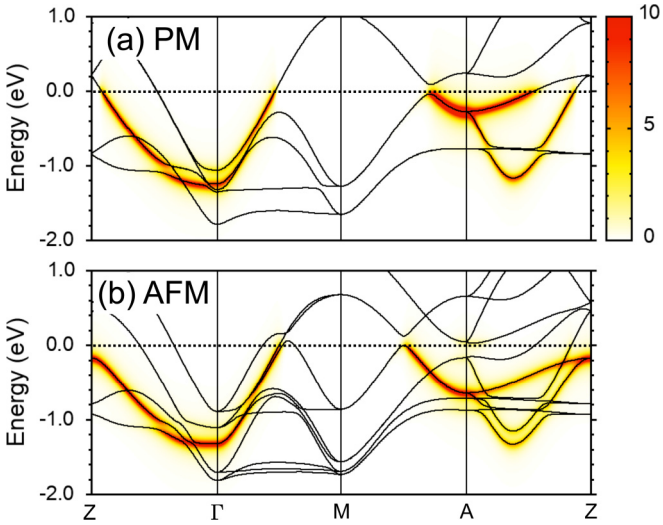

FIG. 3. (a) Paramagnetic and (b) antiferromagnetic band structure obtained with the HF method. Here the SOC is included. The color map shows simulated ARPES spectra. Lorentzian broadening of half-width 0.05 eV and Fermi-Dirac distribution at 300 K are included.

Apart from spin polarization, the AFM order causes changes of the band structure that can be detected with angle-resolved photoemission spectroscopy (ARPES). In Ref. [17], soft x-ray ARPES spectra obtained with p-polarized light were reported. We have simulated p-polarized ARPES spectra, assuming that the scattering plane is perpendicular to the c axis. The resulting spectra in the NM and AFM states are shown in Fig. 3. The spectra along AM and $M\Gamma$ directions agree well with those of Fig. S3 of Ref. [17], while the weaker signal observed observed halfway between Γ and Z should be silent according to our simulation [19]. Comparison of the NM and AFM bands reveals a sizable shift of the FS crossing point on MA with the onset of AFM order, while the crossing point on ΓM moves only slightly. The sharp experimental band observed along MA line does not produce any spin contrast. On the other hand, well-separated spin polarized bands predicted along the AZ line by the present calculation have vanishing cross section for the p polarization of incoming photons.

B. Origin of AFM instability

Similarity between the DMFT and HF results allows us to use the simpler HF approach to analyze the origin of AFM instability. The grand potential in the HF approach with mean-field Δ is given by the sum of the eigenenergies $\epsilon^{\Delta}_{nk,\sigma}$ of occupied single-particle states of the mean-field Hamiltonian (measured from the chemical potential) and a positive Δ-dependent constant $\langle\Omega_{\rm MF}\rangle = \sum_{nk,\sigma}\epsilon^{\Delta}_{nk,\sigma}f_{nk,\sigma} + C(\Delta)$, where $f_{nk,\sigma}$ is the occupation number. The AFM state is stabilized if lowering of the first term overcomes the increase of the second one relative to the NM solution. To assess how different parts of BZ contribute to stabilization of the AFM order, we plot the difference $\eta(k) = \sum_{n,\sigma}(\epsilon^{NM}_{nk,\sigma} - \epsilon^{AFM}_{nk,\sigma})f_{nk,\sigma}$ in Fig. 4. We find a hot spot around the point marked K_2, which extends horizontally toward the zone center. This observation contrasts

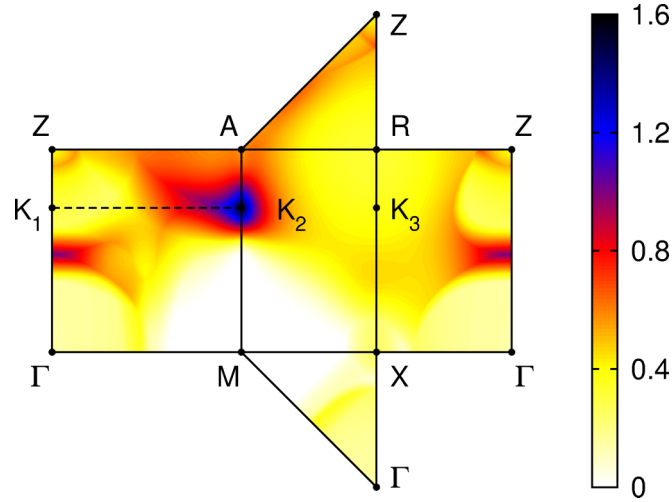

FIG. 4. The contribution $\eta(k)$ (defined in the text) to the condensation energy along several cuts through BZ.

with the result of Ref. [5] where a point on the RX line was identified as a hot spot destabilizing the paramagnetic phase. Large contributions to condensation energy are expected from regions where gaps open at the Fermi level. This is the case of the vicinity of K_2, analyzed in Fig. 5.

At the point K_2 the nodal line NDL1 of Ref. [17] reaches the edge of BZ. Together with the band sticking along vertical faces of BZ, this gives rise to a fourfold degenerate point, which happens to be very close to the Fermi level. The band structure in the vicinity of MA line has a simple explanation in terms of interatomic hopping. The relevant electronic states

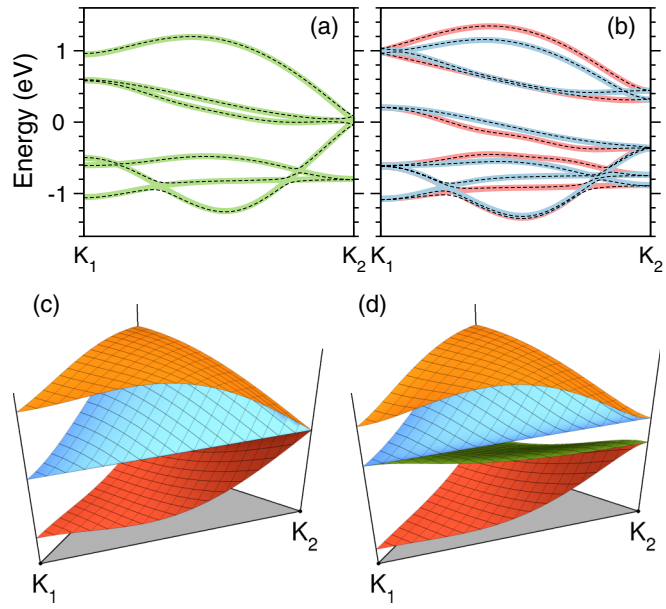

FIG. 5. Band structures along K_1K_2 line of the HF model with (a) the paramagnetic (green) and (b) the AFM (↑ red; ↓ blue) phase. The effect of SOC is represented with dashed (black) lines. (c) Paramagnetic band structure in the horizontal $K_1K_2K_3$ plane obtained with dominant nn hopping. (d) The same as in panel (c) with a staggered potential.

are formed by zx and yz orbitals in the local coordinates shown in Fig. 2(c). Along the MA line the two Ru sites as well as zx and yz orbitals are decoupled and the dispersion is governed by hopping along chains of edge sharing RuO_6 octahedra stretching along the c axis. The opposite sign of zx-zx and yz-yz hopping results in the crossing of the corresponding bands at K_2. The different parity of the zx and yz bands with respect to c-axis inversion explains their appearance and/or absence in the ARPES spectrum of Ref. [17].

The dispersion in $K_1K_2K_3$ plane is governed by the intersublattice Ru_1-Ru_2 hopping (see SM [18] for details). The nodal line NDL1 that is flat connecting K_1 and K_2 points in the nn approximations, Fig. 5(c), acquires some corrugation when long-range hopping and x^2-y^2 orbitals are included; see Fig. 5(a) and Ref. [17]. The AFM order introduces a staggered potential with opposite sign in each spin channel. Its effect on HF bands along K_1K_2 line is shown in Fig. 5(b) (both spin channels) and on the model bands in Fig. 5(d) (one spin channel). The gap opening by the staggered potential can be illustrated by expanding the tight-binding Hamiltonian to linear order around $K_2=(\pi,\pi,z)$,

$$h(\mathbf{k}) = \begin{pmatrix} \Delta+\alpha k_c & 0 & 0 & \gamma(k_a-k_b) \\ 0 & \Delta-\beta k_c & \gamma(k_a+k_b) & 0 \\ 0 & \gamma^*(k_a+k_b) & -\Delta+\alpha k_c & 0 \\ \gamma^*(k_a-k_b) & 0 & 0 & -\Delta-\beta k_c \end{pmatrix}, \tag{1}$$

in the basis formed by $yz(1)$, $zx(1)$, $yz(2)$, and $zx(2)$ orbitals.

To open a gap by the staggered potential Δ, we need a (approximate) band crossing close to the Fermi level and hybridization between the magnetic sublattices (Ru_1-Ru_2) so that the band crossing is not just shifted to a different position in BZ. Such a band structure, described by Eq. (1), is found in the vicinity of NDL1. In the NM state, such k regions are characterized by rapid changes in the Ru_1/Ru_2 sublattice composition of the wave functions. In Fig. 2(a), we show the NM FS colored by the sublattice polarization (difference between Ru_1 and Ru_2 weight) of the corresponding wave functions. The hot spots in Fig. 4 correlate with red and blue boundaries in Fig. 2(a), where sublattice polarized bands meet. The sublattice polarization descends to a spin polarization in the AFM phase [Fig. 2(b)]. On the other hand, the regions with 50:50 sublattice participation are insensitive to the staggered potential, e.g., in the ΓXM plane, and NM and AFM FS essentially coincide with each other.

Finally, we discuss the role of SOC. The band structure calculations of Ref. [17] found a minor modifications of the band structure in the form of avoided band crossings. We find that gapping NDL1 due to SOC has only minor effect on the AFM instability. The impact on the HF band structure depends strongly on the type of mean-field decoupling, a deficiency that is not present in DMFT treatment. In the present work, we have added SOC *a posteriori* to the converged HF, which has the similar effect as in DFT calculation [17]. The band structures with and without SOC are compared in Fig. 5. The main effect of SOC is to break the spin isotropy reflected in magnetocrystalline anisotropy. The HF+SOC calculations yield Ru moments parallel to the c axis.

The rutile structure of RuO_2 gives rise to several interesting phenomena. Šmejkal *et al.* [20] recently suggested realization of crystalline Hall effect in this material. The d-wave modulation of FS results in a finite longitudinal spin conductivity with a sign change between (1,1,0) and (1,−1,0) directions. Another interesting question is the response of the AFM structure to the external magnetic field. Using the weak-coupling approach, the authors of Ref. [7] concluded that the order parameter (staggered moment in this case) aligns parallel to the external field. This is associated with an expansion of FS for the parallel spin component and shrinking of the antiparallel one, with the consequence of breaking the fourfold symmetry in the charge channel. Such behavior of an antiferromagnet would be rather unusual and require extremely soft magnetic moments. We have investigated this possibility with HF calculations (without SOC) but found the conventional behavior with moments turning perpendicular to the external field with a small tilt into the field direction, in which case the $\pi/2$ symmetry between the spin-up and spin-down FS is reserved.

IV. CONCLUSIONS

We have studied the antiferromagnetism of RuO_2 using combinations of DFT band structure with HF and DMFT treatment of intra-atomic interaction. The AFM ordering in RuO_2 has the symmetry of a spin-triplet d-wave Pomeranchuk instability of FS. Unique among common antiferromagnets, the band structure of RuO_2 is spin polarized with the spin-up and spin-down bands connected by $\pi/2$ rotation. This leads to a finite longitudinal spin-conductivity in the ab plane, which has maximal values of opposite signs along the (1,1,0) and (1,−1,0) and zeros along the (1,0,0) and (0,1,0) directions. Reversing the sublattice magnetization switches the sign of the longitudinal spin conductivity and thus can be used to distinguish the antiferromagnetic states with opposite Néel vector.

The origin of AFM instability was traced to a nodal line that accidentally appears close to the Fermi level, gapping of which stabilizes the AFM state. The spin-orbit coupling gives rise to a magnetocrystalline anisotropy, which favors local Ru moments parallel to the c axis, in agreement with the experiment.

ACKNOWLEDGMENTS

The authors thank W. E. Pickett, J. Železný, L. Šmejkal, and K. Yamagami for valuable discussions. K.H.A. and K.W.L. are supported by National Research Foundation (NRF) of Korea Grants No. NRF-2016R1A2B4009579 and No. NRF-2019R1A2C1009588. A.H. and J.K. are supported by the European Research Council (ERC) under the European Union Horizon 2020 research and innovation programme (Grant Agreement No. 646807-EXMAG). Access to computing and storage facilities provided by the Vienna Scientific Cluster (VSC) is greatly appreciated.

[1] P. Wadley, B. Howells, J. Železný, C. Andrews, V. Hills, R. P. Campion, V. Novák, K. Olejník, F. Maccherozzi, S. S. Dhesi, S. Y. Martin, T. Wagner, J. Wunderlich, F. Freimuth, Y. Mokrousov, J. Kuneš, J. S. Chauhan, M. J. Grzybowski, A. W. Rushforth, K. Edmond, B. L. Gallagher, and T. Jungwirth, Science **351**, 587 (2016).

[2] Y. Kamihara, T. Watanabe, M. Hirano, and H. Hosono, J. Am. Chem. Soc. **130**, 3296 (2008).

[3] P. Wadley, V. Novák, R. P. Campion, C. Rinaldi, X. Martí, H. Reichlová, J. Zelezný, J. Gazquez, M. A. Roldan, M. Varela, D. Khalyavin, S. Langridge, D. Kriegner, F. Máca, J. Masek, R. Bertacco, V. Holý, A. W. Rushforth, K. W. Edmonds, B. L. Gallagher, C. T. Foxon, J. Wunderlich, and T. Jungwirth, Nat. Commun. **4**, 2322 (2013).

[4] J. C. Slater, Phys. Rev. **82**, 538 (1951).

[5] T. Berlijn, P. C. Snijders, O. Delaire, H.-D. Zhou, T. A. Maier, H.-B. Cao, S.-X. Chi, M. Matsuda, Y. Wang, M. R. Koehler, P. R. C. Kent, and H. H. Weitering, Phys. Rev. Lett. **118**, 077201 (2017).

[6] Z. H. Zhu, J. Strempfer, R. R. Rao, C. A. Occhialini, J. Pelliciari, Y. Choi, T. Kawaguchi, H. You, J. F. Mitchell, Y. Shao-Horn, and R. Comin, Phys. Rev. Lett. **122**, 017202 (2019).

[7] C. Wu, K. Sun, E. Fradkin, and S.-C. Zhang, Phys. Rev. B **75**, 115103 (2007).

[8] P. Blaha, K. Schwarz, G. K. H. Madsen, D. Kvasnicka, and J. Luitz, *WIEN2K, An Augmented Plane Wave + Local Orbitals Program for Calculating Crystal Properties* (Karlheinz Schwarz, Technische Universität Wien, Wien, Austria, 2001).

[9] J. Kuneš, R. Arita, P. Wissgott, A. Toschi, H. Ikeda, and K. Held, Comput. Phys. Commun. **181**, 1888 (2010).

[10] A. A. Mostofi, J. R. Yates, G. Pizzi, Y.-S. Lee, I. Souza, D. Vanderbilt, and N. Marzari, Comput. Phys. Commun. **185**, 2309 (2014).

[11] J. C. Slater, *Quantum Theory of Atomic Structure* (McGraw-Hill, New York, 1960).

[12] J. Kanamori, Prog. Theor. Phys. **30**, 275 (1963).

[13] P. Werner, A. Comanac, L. de' Medici, M. Troyer, and A. J. Millis, Phys. Rev. Lett. **97**, 076405 (2006).

[14] L. Boehnke, H. Hafermann, M. Ferrero, F. Lechermann, and O. Parcollet, Phys. Rev. B **84**, 075145 (2011).

[15] H. Hafermann, K. R. Patton, and P. Werner, Phys. Rev. B **85**, 205106 (2012).

[16] A. Hariki, A. Yamanaka, and T. Uozumi, J. Phys. Soc. Jpn. **84**, 073706 (2015).

[17] V. Jovic, R. J. Koch, S. K. Panda, H. Berger, P. Bugnon, A. Magrez, K. E. Smith, S. Biermann, C. Jozwiak, A. Bostwick, E. Rotenberg, and S. Moser, Phys. Rev. B **98**, 241101(R) (2018).

[18] See Supplemental Material at http://link.aps.org/supplemental/10.1103/PhysRevB.99.184432 for computational details, magnetic moment in a wide range of U and J parameters, comparison of DFT+U, HF and DMFT approaches, and intersublattice Ru_1-Ru_2 hopping, which includes Refs. [21–26].

[19] This discrepancy could arise from complexities of the matrix-element effects (e.g., photon energy dependence) in ARPES spectra or surface effects. In the present simulation, the selection rule for the orbital excitation under the scattering plane perpendicular to the c axis and p-polarized x-rays is taken into account.

[20] L. Šmejkal, R. González-Hernández, T. Jungwirth, and J. Sinova, arXiv:1901.00445.

[21] J. P. Perdew, K. Burke, and M. Ernzerhof, Phys. Rev. Lett. **77**, 3865 (1996).

[22] V. I. Anisimov, I. V. Solovyev, M. A. Korotin, M. T. Czyżyk, and G. A. Sawatzky, Phys. Rev. B **48**, 16929 (1993).

[23] M. Jarrell and J. Gubernatis, Phys. Rep. **269**, 133 (1996).

[24] X. Wang, E. Gull, L. de' Medici, M. Capone, and A. J. Millis, Phys. Rev. B **80**, 045101 (2009).

[25] J. Mravlje, M. Aichhorn, and A. Georges, Phys. Rev. Lett. **108**, 197202 (2012).

[26] A. Hariki, A. Hausoel, G. Sangiovanni, and J. Kuneš, Phys. Rev. B **96**, 155135 (2017).